JACS Au
AN OPEN ACCESS JOURNAL OF THE AMERICAN CHEMICAL SOCIETY

pubs.acs.org/jacsau

Article

Conversion of Methane with Oxygen to Produce Hydrogen Catalyzed by Triatomic Rh_3^- Cluster Anion

Yi Ren,[†] Yuan Yang,[†] Yan-Xia Zhao,* and Sheng-Gui He

Cite This: *JACS Au* 2022, 2, 197–203

Read Online

ACCESS | Metrics & More | Article Recommendations | Supporting Information

ABSTRACT: Metal catalysts, especially noble metals, have frequently been prepared upon downsizing from nanoparticles to subnanoclusters to catalyze the important reaction of partial oxidation of methane (POM) in order to optimize the catalytic performance and conserve metal resources. Here, benefiting from mass spectrometric experiments in conjunction with photoelectron spectroscopy and quantum chemical calculations, we successfully determine that metal cluster anions composed of only three Rh atoms (Rh_3^-) can catalyze the POM reaction with O_2 to produce $2H_2$ + CO_2 under thermal collision conditions (~300 K). The interdependence between CH_4 and O_2 to protect Rh_3^- from collapse and to promote conversion of $CH_4 \rightarrow 2H_2$ has been clarified. This study not only provides a promising metal cluster displaying good catalytic behavior in POM reaction under mild conditions but also reveals a strictly molecular-level mechanism of direct partial oxidation for the production of hydrogen, a promising renewable energy source in the 21st century.

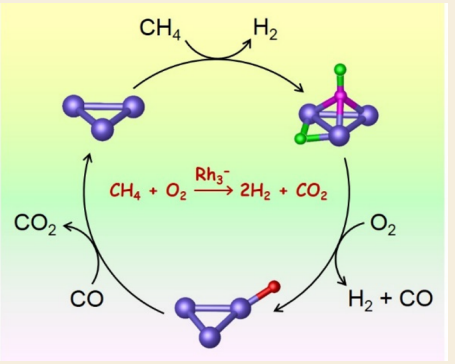

KEYWORDS: *methane, partial oxidation, rhodium clusters, mass spectrometry, quantum chemistry calculations*

1. INTRODUCTION

Hydrogen, a clean and renewable energy source, is of great practical importance for fuel cells as well as the synthesis of chemicals such as ammonia, methanol, and Fischer–Tropsch products.[1−4] Nowadays, the feedstock of natural abundant methane, with a high H/C ratio, accounts for 48% of industrial hydrogen production through steam reforming of methane (SRM),[5] the reaction of which is highly endothermic and energy-intensive. Contrary to the SRM reaction, the partial oxidation of methane (POM) that follows the reaction of CH_4 + O_2 → $2H_2$ + CO_2 enables the generation of highly exothermic H_2 (ΔH_{298} = −3.31 eV) and it is considered as a promising strategy to yield H_2 from an economical perspective.[6,7] However, limited by the inertness of CH_4 and O_2 molecules, the spontaneous POM reaction could occur only at high temperatures (T > 700 °C) in the absence of a catalyst.[8] Since the first experimental detection of free H_2 from POM reaction catalyzed by Ni/Al_2O_3 in 1929,[9] various heterogeneous catalysts supported with base and precious metals have been engineered for CH_4 conversion at relatively low temperatures.[10−14] The dominant size-dependent catalytic behavior of supported metals motivates elaborate controls of metal species spanning from nanoparticles to subnanoclusters, aiming for optimization of the catalytic performance toward the POM reaction and the conservation of metal resources particularly for precious metals (e.g., supported rhodium catalysts with sizes of 30.5 nm → 2.5 nm → 1.3 nm → 0.6 nm have been tailored).[15−18] However, it remains challenging experimentally to achieve catalytic hydrogen production under mild conditions. The genuine mechanisms of H_2 production from POM reaction have also not been completely clarified at a strictly molecular level.

Mass spectrometry coupled with the mass selection technique provides a unique approach to distinguish the atomically precise metal clusters in the gas phase and to explore the intrinsic reactivity property of size-specific metal clusters under isolated conditions.[19−26] Available experiments demonstrated that base metal clusters are commonly unreactive with CH_4 under thermal collision conditions.[27−29] Although most of the unary base metal clusters (M_x^q) could be facilely oxidized by O_2, the generated oxide clusters ($M_xO_y^q$) possessing active sites such as oxygen-centered radicals[19,22] and Lewis acid–base pairs $M^{\delta+}$–$O^{\delta-}$[22] are capable of bringing about thermal methane activation, the process of which generally results in $M_xO_yH_z^q$ product that are difficult to reform back to M_x^q. Although the noble metal clusters ($NM_{x>2}^q$) are able to dehydrogenate methane under thermal collision conditions,[30−32] the catalytic cycle for the reaction of CH_4 with O_2 mediated by metal clusters has not been experimentally identified. So far, only the positively charged atomic Pt^+ as well as diatomic Au_2^+ and PtO^+ were reported to

Received: October 21, 2021
Published: December 3, 2021

https://doi.org/10.1021/jacsau.1c00469
JACS Au 2022, 2, 197–203

catalyze the conversion of CH_4 with O_2 at room temperature.[33,34] Among these catalytic reactions, only the Pt^+ system can convert one CH_4 molecule to generate one H_2 molecule, whereas both of Au_2^+ and PtO^+ convert CH_4 and O_2 to produce formaldehyde and water. Note that three CH_4 molecules were required to complete the catalytic cycle for the Au_2^+ system. Herein, we report the first experimental identification that the thermal reaction of one CH_4 molecule with O_2 to produce two H_2 molecules can be achieved by using a Rh_3^- cluster as a catalyst.

2. RESULTS AND DISCUSSION

Cluster Reactivity

The reactions of laser ablation generated Rh_3^- cluster anions with CH_4 and O_2 were studied by double ion trap experiments in which methane and molecular oxygen were spatially separated by using two ion trap reactors. After thermalization of the mass-selected Rh_3^- anions by collision with He atoms in the first reactor (Figure 1a), CH_4 was injected and reacted for about 3.6 ms. It can be seen from Figure 1b that although the Rh_3^- anions depleted significantly at the CH_4 pressure of 83 mPa, a new strong peak assigned as $Rh_3CH_2^-$ appeared, suggesting that the dehydrogenation of methane with the loss of one H_2 molecule took place (reaction 1):

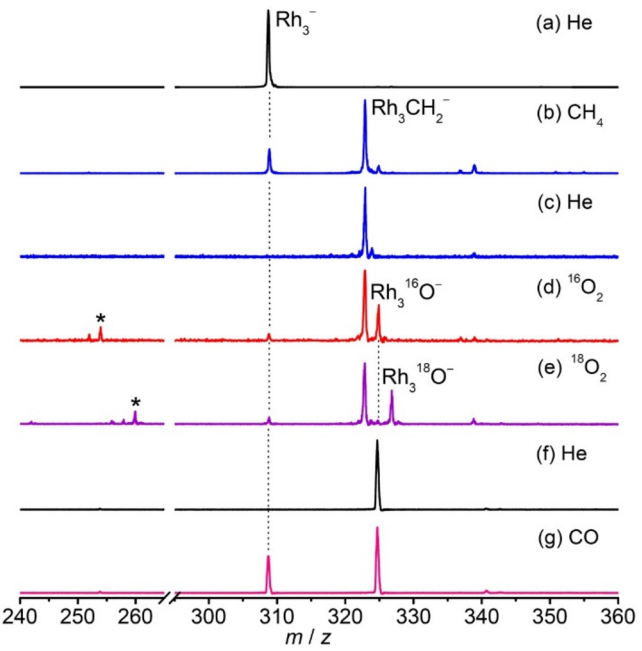

Figure 1. Mass spectra for the reactions of mass-selected Rh_3^- with (a) He and (b) 83 mPa CH_4; $Rh_3CH_2^-$ with (c) He, (d) 1.33 mPa $^{16}O_2$, and (e) 1.05 mPa $^{18}O_2$; and Rh_3O^- with (f) He and (g) 0.7 mPa CO under thermal collision conditions. The reaction times are (b) 3.6 ms, (d, e) 1.9 ms, and (g) 3.6 ms. The peaks marked with asterisks in panels d and e can be assigned to $Rh_2O_3^-$ originating from the oxidation of Rh_3O^- by O_2 (Figure S1).

$$Rh_3^- + CH_4 \rightarrow Rh_3CH_2^- + H_2 \quad (1)$$

The isotopic labeling experiment with CD_4 confirmed the dehydrogenation channel (Figure S1). The rate constant (k_1) of a pseudo-first-order reaction between Rh_3^- and CH_4 was determined to be 1.9×10^{-11} cm^3 $molecule^{-1}$ s^{-1},[35,36] corresponding to a reaction efficiency of 1.9%. The kinetic isotopic effect ($k_{1,CH4}/k_{1,CD4}$) was estimated to be 7.9.

After Rh_3^- reacted with CH_4 in the first reactor, the resulting product ions $Rh_3CH_2^-$ were then mass-selected (Figure 1c) and thermalized in the second reactor for reaction with O_2. As shown in Figure 1d, upon the interaction of $Rh_3CH_2^-$ with 1.33 mPa $^{16}O_2$ for about 1.9 ms, a strong product peak with the mass larger than that of $Rh_3CH_2^-$ by 2 amu emerged and it can be assigned as $Rh_3{}^{16}O^-$, which was further confirmed by the isotopic labeling experiment with $^{18}O_2$ (Figure 1e). In addition, a weak product signal corresponding to Rh_3^- was clearly identified. Two possible channels could be considered for the generation of Rh_3O^- or Rh_3^- in the reaction of $Rh_3CH_2^-$ with O_2. The Rh_3O^- could be produced by either the successive desorption of H_2 and CO molecules (reaction 2a) or the direct evaporation of a CH_2O molecule (reaction 2b). Likewise, the successive liberation of H_2 and CO_2 molecules results in the formation of Rh_3^- (reaction 3a). The Rh_3^- may also originate from the evaporation of CH_2O_2 (reaction 3b).

$$Rh_3CH_2^- + O_2 \rightarrow Rh_3O^- + H_2 + CO \quad (2a)$$

$$\rightarrow Rh_3O^- + CH_2O \quad (2b)$$

$$\rightarrow Rh_3^- + H_2 + CO_2 \quad (3a)$$

$$\rightarrow Rh_3^- + CH_2O_2 \quad (3b)$$

Further theoretical calculations (see below) support that the Rh_3O^- and Rh_3^- are more likely to be generated through the channels involving liberation of H_2 and CO/CO_2 molecules (reactions 2a and 3a). The measured $k_1(Rh_3CH_2^- + O_2)$ is 7.2×10^{-10} cm^3 $molecule^{-1}$ s^{-1} that is larger than $k_1(Rh_3^- + CH_4)$ by more than 1 order of magnitude.

Further experiments demonstrated that the produced Rh_3O^- (Figure 1f) in reaction 2a could be very efficiently reduced to Rh_3^- by CO (Figure 1g and reaction 4) with k_1 of 1.6×10^{-9} cm^3 $molecule^{-1}$ s^{-1}. As a result

$$Rh_3O^- + CO \rightarrow Rh_3^- + CO_2 \quad (4)$$

on the basis of reactions 1, 2a, 3a, and 4, it can be concluded that the reaction of CH_4 with O_2 can produce two H_2 molecules with concomitant formation of CO_2 under thermal collision conditions catalyzed by the Rh_3^- cluster. Furthermore, two pathways (i and ii) to complete the catalytic cycle are identified at a strictly molecular level, as shown in Figure 2.

Structures of Reaction Intermediates and Reaction Mechanisms

The ground-state structure of Rh_3^- cluster was previously characterized to have an isosceles triangle in the quintet state.[35,37] To explore the mechanistic details for the reaction of CH_4 with O_2 catalyzed by Rh_3^-, we conducted the photoelectron spectroscopy (PES) experiments and density functional theory (DFT) calculations with PBE functional[38] in an attempt to determine the structures of the important reaction intermediates $Rh_3CH_2^-$ and Rh_3O^- involved in the catalytic cycles. The comparison between experimental PES spectra and simulated density of states (DOS) spectra of isomeric structures (Figure 3, Figures S3 and S4) shows that (i) the structure of $Rh_3CH_2^-$ can be in the triplet $HRh_3(CH)^-$ by capping a C−H unit on the top of the Rh_3 plane and suspending the second H atom by two Rh atoms; (ii) the

https://doi.org/10.1021/jacsau.1c00469
JACS Au 2022, 2, 197−203

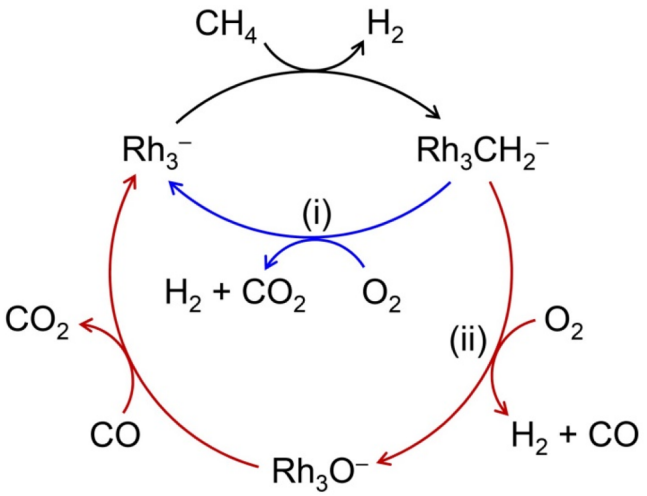

Figure 2. Proposed catalytic cycles for the reaction of $CH_4 + O_2 \rightarrow 2H_2 + CO_2$ mediated by Rh_3^- cluster.

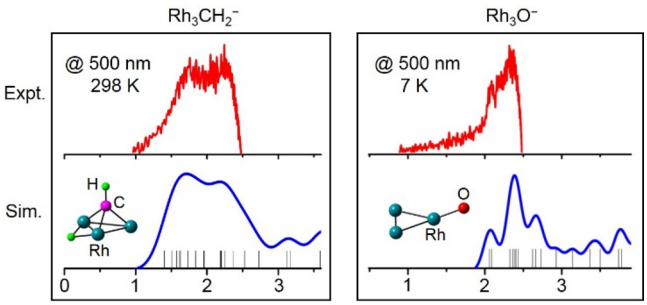

Figure 3. Experimental (Expt.) photoelectron spectra and simulated (Sim.) density of states (DOS) spectra for isomers of $Rh_3CH_2^-$ (left) and Rh_3O^- (right). The DOS spectrum for Rh_3O^- is red-shifted by 0.08 eV. Both the DFT calculated isomers of $Rh_3CH_2^-$ and Rh_3O^- are in the triplet state.

Rh_3O^- is also in a triplet state that possesses an O atom terminally attached to one Rh atom of the Rh_3 moiety.

The most possible pathways computed with DFT method for the elementary reactions of Rh_3^- with CH_4 (R1) and $Rh_3CH_2^-$ with O_2 (R2) are shown in Figures 4 and S5–S8. The quintet Rh_3^- traps CH_4 by one Rh atom (Rh_α) to form encounter complex I1 with a binding energy of 0.20 eV. The oxidative addition of the first C–H bond onto Rh_α then takes place with a small energy barrier of 0.12 eV (^{5}I1 → ^{5}TS1), resulting in formation of the $CH_3–Rh_\alpha–H–Rh_\beta$ moiety. After the bridging H atom (H_b) moves away from Rh_α (^{5}I2 → ^{5}I3, Figure S5), the CH_3 moiety that has been bonded with Rh_α also connects to the Rh_γ atom (^{5}I3 → ^{5}I4) so that the second and the third C–H bonds can be successively activated by Rh_α (I4 → TS4 → I5) and Rh_γ (I5 → TS5 → I6), respectively. Note that a spin inversion from quintet state to triplet state occurs during activation of the second C–H bond (^{5}I4 → ^{3}TS4, Figure S6). The facile cleavage of three C–H bonds of CH_4 leads to the formation of a more stable intermediate I6, in which each Rh atom is coordinated with a terminal H atom (H_t). Subsequently, the residual C–H bond in I6 moves toward the Rh_β atom and the most stable intermediate I7 is formed by capping a C–H unit on the top of Rh_3 plane. Meanwhile, two of the three H_t atoms in I6 become H_b atoms in I7. The H_t in I7 then combines with the adjacent H_b to form an H_2 molecule and then desorb from Rh_γ (I7 → I8 → P1), leading to the generation of triplet $Rh_3CH_2^-$ ion.

In the reaction of $^3Rh_3CH_2^-$ with O_2, the spare Rh_γ adsorbs the O_2 molecule to form intermediate ^{3}I9 and 2.55 eV of energy is released. Thus, the ^{3}I9 has enough energy to overcome the barrier (1.05 eV, ^{3}I9 → ^{3}TS8) for cleavage of the O–O bond by cooperation between Rh_γ and Rh_β, resulting in the more stable intermediate ^{3}I10 with an O_t and an O_b attached to Rh atoms. The ^{3}I10 then undergoes a series of structural rearrangements involving H_t transfer from Rh_α to Rh_β (I10 → I11, Figure S7) and rupture of the HC–Rh_γ bond (I11 → I12). Subsequently, the HC–O_b coupling (^{3}I12 → ^{3}I13) occurs, followed by activation of the fourth C–H bond by Rh_α (^{3}I13 → ^{3}I14 → ^{3}I15) and formation of ^{3}I15 that has two H_t atoms coordinated with Rh_α and Rh_β. After the H_t originally bonded with Rh_α transfers to Rh_β (^{3}I15 → ^{3}I16 → ^{3}I17 → ^{3}I18), the two H_t atoms on Rh_β in ^{3}I18 could make an H_2 unit and are finally evaporated to form triplet $Rh_3CO_2^-$ (^{3}I19), the structure of which contains an isolated CO unit and an O_t atom.

It is noteworthy that the production of H_2 in the reaction of $^3Rh_3CH_2^- + O_2$ is highly exothermic (by 4.59 eV) so the resulting $^3Rh_3CO_2^-$ possesses sufficient internal energy to enable the CO desorption and generation of triplet Rh_3O^- ion (I19 → Rh_3O^- + CO, P2). Alternatively, the CO moiety in $^3Rh_3CO_2^-$ could directly couple with the O_t atom to form a CO_2 unit, which is further evaporated to reform quintet Rh_3^- through a spin conversion (^{3}I19 → ^{3}I20 → ^{3}I21 → ^{5}I22 → ^{5}I23 → $^5Rh_3^- + CO_2$, P3, Figures S7 and S8). Despite that the channel of CO_2 elimination ($\Delta H_0 = -2.52$ eV) is thermodynamically more favorable than that of CO desorption ($\Delta H_0 = -1.66$ eV), the kinetic analysis on the basis of Rice–Ramsperger–Kassel–Marcus (RRKM) theory[39] demonstrates that the rate (6.1×10^{10} s^{-1}) of CO desorption from $Rh_3CO_2^-$ is about six times the rate of internal conversion (1.0×10^{10} s^{-1}) of I19 → TS19 involved in CO_2 formation. Thus, the reaction of $Rh_3CH_2^-$ with O_2 should generate Rh_3O^- + CO (rather than $Rh_3^- + CO_2$) as the major product, in consistent with the experimental observation (Figures 1d, e). The pathway for direct elimination of CH_2O to produce Rh_3O^- was also considered for the reaction of $Rh_3CH_2^- + O_2$ (Figure S9); however, it is kinetically less favorable than the path of H_2 + CO production. The $^3Rh_3O^-$ generated after H_2 + CO desorption can further barrierlessly adsorb and oxidize a CO molecule to CO_2, and $^3Rh_3O^-$ is reduced to $^5Rh_3^-$ following the same path as I20 → P3. As a result, the computational results support the idea that the reaction of CH_4 with O_2 to produce $2H_2 + CO_2$ can be achieved under thermal collision conditions using a Rh_3^- catalyst.

Insights into the Gas-Phase Catalysis and Related Condensed-Phase Catalysis

The transformation of important molecules with molecular oxygen mediated by atomic clusters has received considerable attention in gas-phase studies, but only a very limited number of bare metal clusters including Pt_{3-6}^-,[40] Au_6^-,[41] and $Ag_{7,9,11}^-$[42] have been reported to exhibit catalytic behavior. The elaborate measurement on elementary reactions demonstrated that the completion of catalytic cycles requires preferential adsorption of O_2 onto M_x^- clusters and the resulting $M_xO_y^-$ then oxidizes small molecules (e.g., CO) to reform M_x^-. In this study, we identify the first example for catalytic conversion of CH_4 with O_2 mediated by a metal

https://doi.org/10.1021/jacsau.1c00469
JACS Au 2022, 2, 197–203

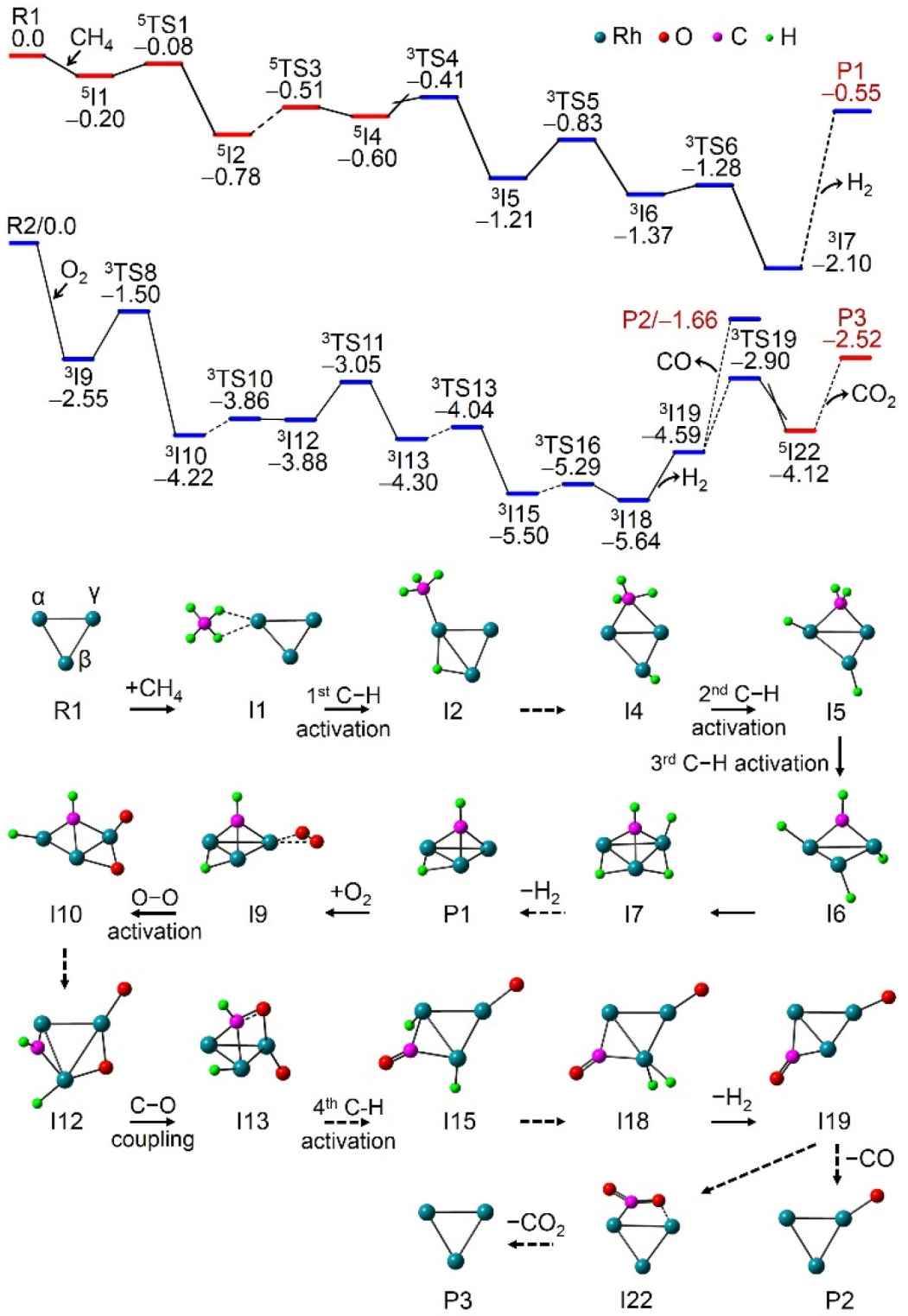

Figure 4. DFT calculated potential energy profiles for reactions of $^5Rh_3^-$ + CH_4 (R1) and $^3Rh_3CH_2^-$ + O_2 (R2). The relative energies (ΔH_0) are given in eV. The structures of R, I1, I2, I4−I7, I9, I10, I12, I13, I15, I18, I19, I22, P1 ($^3Rh_3CH_2^-$ + H_2), P2 ($^3Rh_3O^-$ + H_2 + CO), and P3 ($^5Rh_3^-$ + H_2 + CO_2) are plotted, whereas those of I3, I8, I11, I14, I16, I17, I20, I21, I23, and TS1−TS20 can be found in the Supporting Information. The superscript denotes the spin multiplicity.

cluster (Rh_3^-), moreover, a distinct mechanism to complete the catalytic cycle has been definitely determined. The Rh_3^- should react with CH_4 at first to produce $Rh_3CH_2^-$ + H_2, after which O_2 is dissociatively adsorbed onto the $Rh_3CH_2^-$ intermediate, enabling formation of the second H_2 molecule and CO_2 as well as regeneration of Rh_3^- cluster. The preferential oxidation of Rh_3^- by O_2 has also been experimentally tested. Unfortunately, the Rh_3^- rapidly disintegrates into $Rh_2O_2^-$ + Rh and RhO_2^- + Rh_2 with k_1 of 7.1 × 10^{-10} cm^3 $molecule^{-1}$ s^{-1} (Figures S1 and S2). The

https://doi.org/10.1021/jacsau.1c00469
JACS Au 2022, 2, 197−203

stepwise reaction of Rh_3^- with CH_4 and then with O_2 to close the catalytic cycle for production of $2H_2 + CO_2$ (Figure 2) thus implies an interdependence between CH_4 and O_2 that the preferential reaction with CH_4 could protect Rh_3^- cluster from collapse, whereas the O_2 adsorption could promote transformation of CH_4 to two H_2 molecules afterward.

The fundamental mechanism of the POM reaction with molecular oxygen over bulk Rh-based catalysts has been extensively investigated. Some researchers studying the catalysts of supported rhodium nanoparticles or nanoclusters (with the sizes of 0.6−3.3 nm) proposed that the H_2 (and CO) production follows a combustion-reforming mechanism,[15−18] among which CH_4 and O_2 first undergo combustion to give CO_2 and H_2O and subsequently the steaming (H_2O) or dry (CO_2) reforming of unreacted methane and water−gas shift reactions occur. Alternatively, the direct partial oxidation mechanism with H_2 (and H_2O) as primary products was emphasized on the Rh(111) single crystal surface.[43] However, there remains a lack of experimental techniques to characterize the elementary steps in condensed-phase systems and to prove the proposed mechanisms. Herein, benefiting from the well-controlled gas phase cluster reactions, we identify that the rhodium cluster composed of only three Rh atoms (Rh_3^-) is active enough to catalyze the POM reaction under thermal collision conditions. Furthermore, the mechanism of direct H_2 production has also been certified at a strictly molecular level by following each elementary step of the catalytic cycle (Figure 2). It is noteworthy that the product H_2 has the possibility of being oxidized into H_2O by the Rh_3O^- ion, the important intermediate generated during the catalytic reaction. Our further mass spectrometric experiments (Figure S1 and S2) demonstrate that the reaction rate (5.3×10^{-10} cm^3 $molecule^{-1}$ s^{-1}) of $Rh_3O^- + H_2$ is slower than that of Rh_3O^- + CO by a factor of 3, which is advantageous for improving the product yield of H_2. The employment of a hydrogen-permeable membrane reactor in real-life catalysis may further allow the selective separation of H_2.[44]

3. CONCLUSION

In summary, the catalytic conversion of CH_4 with O_2 mediated by the atomic cluster Rh_3^- has been experimentally achieved in the gas phase. Although the Rh_3^- cluster is prone to disintegrate upon interaction with O_2, the preferential thermal reaction of Rh_3^- with CH_4 could generate a H_2 molecule and a $Rh_3CH_2^-$ ion. The resulting $Rh_3CH_2^-$ subsequently reacts with O_2 to produce the second H_2 molecule and CO; meanwhile, the intact [Rh_3] moiety is oxidized to Rh_3O^- that can be further reduced by CO to reform Rh_3^-. Thus, the cycle for partial oxidation of CH_4 with O_2 to $2H_2 + CO_2$ is closed by using the Rh_3^- cluster catalyst. This study not only makes a significant step toward catalytic conversion of methane with O_2 mediated by atomic clusters, but also provides molecular evidence for the direct partial oxidation mechanism for H_2 production from methane under mild conditions.

4. METHODS

Experimental Methods

The negatively charged rhodium clusters (Rh_x^-) were generated by laser ablation of a rotating and translating Rh disk in the presence of a 6 atm He carrier gas. The reactivity experiments were carried out in a double ion trap system, which includes two quadrupole mass filters (QMFs) and two linear ion traps (LITs). Among many generated Rh_x^- clusters, the triatomic Rh_3^- ions of interest were mass-selected by using the first QMF[45] and entered into the first LIT reactor,[46] where they were confined and thermalized by collisions with a pulse of buffer gas He and then reacted with $^{12}CH_4$ or CD_4. The second QMF mass-selected the product ions (e.g., $Rh_3CH_2^-$) resulting from the first LIT to inject into the second LIT for further reaction with $^{16}O_2$ or $^{18}O_2$ molecule. The Rh_3O^- cluster was also generated by laser ablation of the Rh disk in the presence of 0.02% $^{16}O_2$/He for reaction with reactant molecules of CO and H_2. The temperature of cooling gas (He), reactant gases, and LIT reactor was around 300 K. A reflectron time-of-flight mass spectrometer[47] was used to detect the cluster ions ejected from the LIT reactor. The photoelectron imaging spectroscopy[48] was employed to characterize the structures of reaction intermediates $Rh_3CH_2^-$ and Rh_3O^-. Details on experimental methods can be found in the Supporting Information.

Theoretical Methods

Density functional theory (DFT) calculations using the *Gaussian 09* program[49] were carried out to investigate the structures of reaction intermediates Rh_3X^- (X = CH_2, CO, O) as well as the reaction pathways of $Rh_3^- + CH_4$, $Rh_3CH_2^- + O_2$, and Rh_3O^- + CO. The PBE functional[38] has been proved to perform well for bare rhodium clusters[35] so the results by PBE method are given throughout this work. The TZVP basis sets[50] for C, H, and O atoms and the D95V basis set combined with the Stuttgart/Dresden relativistic effective core potentials (denoted as SDD in the *Gaussian* software)[51] for Rh atom were used. The reaction pathway calculations involved geometry optimization of reaction intermediates (IMs) and transition states (TSs) through which the IMs transfer to each other. The zero-point vibration corrected energies (ΔH_0) in units of eV are reported in this work. The Rice−Ramsperger−Kassel−Marcus (RRKM) based theory[39] was used to predict the rates of internal conversion of reaction intermediates. The density of states (DOS) simulations based on the generalized Koopmans' theorem[52] were performed to assign the structures of reaction intermediates through comparison with the photoelectron spectra in the experiment. Details on theoretical methods can be found in the Supporting Information.

■ ASSOCIATED CONTENT

Supporting Information

The Supporting Information is available free of charge at https://pubs.acs.org/doi/10.1021/jacsau.1c00469.

Method details and additional experimental and theoretical results (spectra, calculated structures, and reaction pathways) (PDF)

■ AUTHOR INFORMATION

Corresponding Author

Yan-Xia Zhao − *State Key Laboratory for Structural Chemistry of Unstable and Stable Species, Institute of Chemistry, Chinese Academy of Sciences, Beijing 100190, P. R. China; Beijing National Laboratory for Molecular Sciences and CAS Research/Education Centre of Excellence in Molecular Sciences, Beijing 100190, P. R. China;* orcid.org/0000-0002-4425-5211; Email: chemzyx@iccas.ac.cn

Authors

Yi Ren − *State Key Laboratory for Structural Chemistry of Unstable and Stable Species, Institute of Chemistry, Chinese Academy of Sciences, Beijing 100190, P. R. China*

Yuan Yang − *State Key Laboratory for Structural Chemistry of Unstable and Stable Species, Institute of Chemistry, Chinese Academy of Sciences, Beijing 100190, P. R. China*

Sheng-Gui He − *State Key Laboratory for Structural Chemistry of Unstable and Stable Species, Institute of*

https://doi.org/10.1021/jacsau.1c00469
JACS Au 2022, 2, 197−203

Chemistry, Chinese Academy of Sciences, Beijing 100190, P. R. China; Beijing National Laboratory for Molecular Sciences and CAS Research/Education Centre of Excellence in Molecular Sciences, Beijing 100190, P. R. China; University of Chinese Academy of Sciences, Beijing 100049, P. R. China; orcid.org/0000-0002-9919-6909

Complete contact information is available at: https://pubs.acs.org/10.1021/jacsau.1c00469

Author Contributions

†Y.R. and Y.Y. contributed equally.

Notes

The authors declare no competing financial interest.

■ ACKNOWLEDGMENTS

This work was financially supported by the National Natural Science Foundation of China (92061115 and 22173111), the Youth Innovation Promotion Association CAS (2018041), and the K. C. Wong Education Foundation.

■ REFERENCES

(1) Henrici-Olivé, G.; Olivé, S. The Fischer−Tropsch Synthesis: Molecular Weight Distribution of Primary Products and Reaction Mechanism. *Angew. Chem., Int. Ed. Engl.* **1976**, *15*, 136−141.
(2) Navarro, R. M.; Peña, M. A.; Fierro, J. L. G. Hydrogen Production Reactions from Carbon Feedstocks: Fossil Fuels and Biomass. *Chem. Rev.* **2007**, *107*, 3952−3991.
(3) Fan, Z.; Weng, W.; Zhou, J.; Gu, D.; Xiao, W. Catalytic decomposition of methane to produce hydrogen: A review. *J. Energy Chem.* **2021**, *58*, 415−430.
(4) Yan, G.; Gao, Z.; Zhao, M.; Ma, K.; Ding, Z.; Yang, W.; Ding, X. Mechanism study on CO_2 reforming of methane over platinum cluster doped graphene: A DFT calculation. *Mol. Catal.* **2020**, *497*, 111205.
(5) Koumi Ngoh, S.; Njomo, D. An overview of hydrogen gas production from solar energy. *Renewable Sustainable Energy Rev.* **2012**, *16*, 6782−6792.
(6) Christian Enger, B.; Lødeng, R.; Holmen, A. A review of catalytic partial oxidation of methane to synthesis gas with emphasis on reaction mechanisms over transition metal catalysts. *Appl. Catal., A* **2008**, *346*, 1−27.
(7) Elbadawi, A. H.; Ge, L.; Li, Z.; Liu, S.; Wang, S.; Zhu, Z. Catalytic partial oxidation of methane to syngas: review of perovskite catalysts and membrane reactors. *Catal. Rev.: Sci. Eng.* **2021**, *63*, 1−67.
(8) Prettre, M.; Eichner, Ch.; Perrin, M. The Catalytic Oxidation of Methane to Carbon monoxide and Hydrogen. *Trans. Faraday Soc.* **1946**, *42*, 335−340.
(9) Liander, H. The Utilisation of Natural Gases for The Ammonia Process. *Trans. Faraday Soc.* **1929**, *25*, 462−472.
(10) Choudhary, V. R.; Mammon, A. S.; Sansare, S. D. Selective Oxidation of Methane to CO and H_2 over Ni/MgO at Low Temperatures. *Angew. Chem., Int. Ed. Engl.* **1992**, *31*, 1189−1190.
(11) Hickman, D. A.; Schmidt, L. D. Production of Syngas by Direct Catalytic Oxidation of Methane. *Science* **1993**, *259*, 343−346.
(12) Zhu, Y.; Zhang, S.; Shan, J.-j.; Nguyen, L.; Zhan, S.; Gu, X.; Tao, F. In Situ Surface Chemistries and Catalytic Performances of Ceria Doped with Palladium, Platinum, and Rhodium in Methane Partial Oxidation for the Production of Syngas. *ACS Catal.* **2013**, *3*, 2627−2639.
(13) Leclerc, C. A.; Gudgila, R. Short Contact Time Catalytic Partial Oxidation of Methane over Rhodium Supported on Ceria Based 3-D Printed Supports. *Ind. Eng. Chem. Res.* **2019**, *58*, 14632−14637.
(14) Wu, C.; Yang, W.; Wang, J.; Li, H.; Gates, I. D. Methane activation on dual-atom catalysts supported on graphene. *Chem. Commun.* **2021**, *57*, 12127.
(15) Chin, Y.-H.; Buda, C.; Neurock, M.; Iglesia, E. Selectivity of chemisorbed oxygen in C-H bond activation and CO oxidation and kinetic consequences for CH_4-O_2 catalysis on Pt and Rh clusters. *J. Catal.* **2011**, *283*, 10−24.
(16) Berger-Karin, C.; Wohlrab, S.; Rodemerck, U.; Kondratenko, E. V. The tremendous effect of trace amounts of Rh on redox and catalytic properties of CeO_2-TiO_2 and Al_2O_3 in CH_4 partial oxidation. *Catal. Commun.* **2012**, *18*, 121−125.
(17) Kondratenko, V. A.; Berger-Karin, C.; Kondratenko, E. V. Partial Oxidation of Methane to Syngas Over γ-Al_2O_3-Supported Rh Nanoparticles: Kinetic and Mechanistic Origins of Size Effect on Selectivity and Activity. *ACS Catal.* **2014**, *4*, 3136−3144.
(18) Hou, Y.; Ogasawara, S.; Fukuoka, A.; Kobayashi, H. Zeolite-supported rhodium sub-nano cluster catalyst for low-temperature selective oxidation of methane to syngas. *Catal. Sci. Technol.* **2017**, *7*, 6132−6139.
(19) Ding, X.-L.; Wu, X.-N.; Zhao, Y.-X.; He, S.-G. C-H Bond Activation by Oxygen-Centered Radicals over Atomic Clusters. *Acc. Chem. Res.* **2012**, *45*, 382−390.
(20) Luo, Z.; Castleman, A. W.; Khanna, S. N. Reactivity of Metal Clusters. *Chem. Rev.* **2016**, *116*, 14456−14492.
(21) Zhang, X.; Liu, G.; Meiwes-Broer, K.-H.; Ganteför, G.; Bowen, K. CO_2 Activation and Hydrogenation by PtH_n^- Cluster Anions. *Angew. Chem., Int. Ed.* **2016**, *55*, 9644−9647.
(22) Schwarz, H.; Shaik, S.; Li, J. Electronic Effects on Room-Temperature, Gas-Phase C-H Bond Activations by Cluster Oxides and Metal Carbides: The Methane Challenge. *J. Am. Chem. Soc.* **2017**, *139*, 17201−17212.
(23) Li, Y.-K.; Debnath, S.; Schlangen, M.; Schoellkopf, W.; Asmis, K. R.; Schwarz, H. Direct Identification of Acetaldehyde Formation and Characterization of the Active Site in the $[VPO_4]^+/C_2H_4$ Couple by Gas-Phase Vibrational Spectroscopy. *Angew. Chem., Int. Ed.* **2019**, *58*, 18868−18872.
(24) Hirabayashi, S.; Ichihashi, M. Dehydrogenation of Methane by Partially Oxidized Tungsten Cluster Cations: High Reactivity Comparable to That of Platinum Cluster Cations. *J. Phys. Chem. A* **2019**, *123*, 6840−6847.
(25) Yamaguchi, M.; Zhang, Y. F.; Kudoh, S.; Koyama, K.; Lushchikova, O. V.; Bakker, J. M.; Mafuné, F. Oxophilicity as a Descriptor for NO Cleavage Efficiency over Group IX Metal Clusters. *J. Phys. Chem. Lett.* **2020**, *11*, 4408−4412.
(26) Levin, N.; Lengyel, J.; Eckhard, J. F.; Tschurl, M.; Heiz, U. Catalytic Non-Oxidative Coupling of Methane on $Ta_8O_2^+$. *J. Am. Chem. Soc.* **2020**, *142*, 5862−5869.
(27) Nakajima, A.; Kishi, T.; Sone, Y.; Nonose, S.; Kaya, K. Reactivity of positively charged cobalt cluster ions with CH_4, N_2, H_2, C_2H_4, and C_2H_2. *Z. Phys. D: At., Mol. Clusters* **1991**, *19*, 385−387.
(28) Liyanage, R.; Zhang, X.-G.; Armentrout, P. B. Activation of methane by size-selected iron cluster cations, Fe_n^+ (n = 2−15): Cluster-CH_x (x = 0−3) bond energies and reaction mechanisms. *J. Chem. Phys.* **2001**, *115*, 9747−9763.
(29) Liu, F.; Zhang, X.-G.; Liyanage, R.; Armentrout, P. B. Methane activation by nickel cluster cations, Ni_n^+(n = 2−16): Reaction mechanisms and thermochemistry of cluster-CH_x (x = 0−3) complexes. *J. Chem. Phys.* **2004**, *121*, 10976−10990.
(30) Koszinowski, K.; Schlangen, M.; Schröder, D.; Schwarz, H. CH- and NH-activation by gaseous Rh_2^+ and $PtRh^+$ cluster ions. *Int. J. Mass Spectrom.* **2004**, *237*, 19−23.
(31) Adlhart, C.; Uggerud, E. Reactions of platinum clusters $Pt_n^{\pm}$, n = 1−21, with CH_4: to react or not to react. *Chem. Commun.* **2006**, 2581−2582.
(32) Lang, S. M.; Frank, A.; Bernhardt, T. M. Activation and Catalytic Dehydrogenation of Methane on Small Pd_x^+ and Pd_xO^+ Clusters. *J. Phys. Chem. C* **2013**, *117*, 9791−9800.
(33) Wesendrup, R.; Schröder, D.; Schwarz, H. Catalytic Pt^+-Mediated Oxidation of Methane by Molecular Oxygen in the Gas Phase. *Angew. Chem., Int. Ed. Engl.* **1994**, *33*, 1174−1176.
(34) Lang, S. M.; Bernhardt, T. M.; Barnett, R. N.; Landman, U. Temperature-Tunable Selective Methane Catalysis on Au_2^+: From Cryogenic Partial Oxidation Yielding Formaldehyde to Cold Ethylene Production. *J. Phys. Chem. C* **2011**, *115*, 6788−6795.

(35) Ren, Y.; Yang, Y.; Zhao, Y.-X.; He, S.-G. Size-Dependent Reactivity of Rhodium Cluster Anions toward Methane. *J. Phys. Chem. C* **2019**, *123*, 17035−17042.
(36) Zhao, Y.-X.; Zhao, X.-G.; Yang, Y.; Ruan, M.; He, S.-G. Rhodium chemistry: A gas phase cluster Study. *J. Chem. Phys.* **2021**, *154*, 180901.
(37) Beltran, M. R.; Buendia Zamudio, F.; Chauhan, V.; Sen, P.; Wang, H.; Ko, Y. J.; Bowen, K. Ab initio and anion photoelectron studies of Rh_n (n = 1 −9) clusters. *Eur. Phys. J. D* **2013**, *67*, 63.
(38) Perdew, J. P.; Burke, K.; Ernzerhof, M. Generalized Gradient Approximation Made Simple. *Phys. Rev. Lett.* **1996**, *77*, 3865−3868.
(39) Steinfeld, J. I.; Francisco, J. S.; Hase, W. L. *Chemical Kinetics and Dynamics*; Prentice-Hall: Upper Saddle River, NJ, 1999; p 231 and 313.
(40) Shi, Y.; Ervin, K. M. Catalytic oxidation of carbon monoxide by platinum cluster anions. *J. Chem. Phys.* **1998**, *108*, 1757−1760.
(41) Wallace, W. T.; Whetten, R. L. Coadsorption of CO and O_2 on selected gold clusters: Evidence for efficient room-temperature CO_2 generation. *J. Am. Chem. Soc.* **2002**, *124*, 7499−7505.
(42) Socaciu, L. D.; Hagen, J.; Le Roux, J.; Popolan, D.; Bernhardt, T. M.; Woste, L.; Vajda, S. Strongly cluster size dependent reaction behavior of CO with O_2 on free silver cluster Anions. *J. Chem. Phys.* **2004**, *120*, 2078−2081.
(43) Wilson, J. N.; Pedigo, R. A.; Zaera, F. Kinetics and Mechanism of Catalytic Partial Oxidation Reactions of Alkanes on Rhodium Surfaces. *J. Am. Chem. Soc.* **2008**, *130*, 15796−15797.
(44) Uemiya, S.; Sato, N.; Ando, H.; Matsuda, T.; Kikuchi, E. Steam reforming of methane in a hydrogen-permeable membrane reactor. *Appl. Catal.* **1990**, *67*, 223−230.
(45) Yuan, Z.; Zhao, Y.-X.; Li, X.-N.; He, S.-G. Reactions of $V_4O_{10}^+$ cluster ions with simple inorganic and organic Molecules. *Int. J. Mass Spectrom.* **2013**, *354*−*355*, 105−112.
(46) Yuan, Z.; Li, Z.-Y.; Zhou, Z.-X.; Liu, Q.-Y.; Zhao, Y.-X.; He, S.-G. Thermal Reactions of $(V_2O_5)_nO^-$ (n = 1−3) Cluster Anions with Ethylene and Propylene: Oxygen Atom Transfer Versus Molecular Association. *J. Phys. Chem. C* **2014**, *118*, 14967−14976.
(47) Wu, X.-N.; Xu, B.; Meng, J.-H.; He, S.-G. C-H bond activation by nanosized scandium oxide clusters in gas-phase. *Int. J. Mass Spectrom.* **2012**, *310*, 57−64.
(48) Liu, Q.-Y.; Hu, L.; Li, Z.-Y.; Ning, C.-G.; Ma, J.-B.; Chen, H.; He, S.-G. Photoelectron imaging spectroscopy of MoC^- and NbN^- diatomic anions: A comparative study. *J. Chem. Phys.* **2015**, *142*, 164301.
(49) Frisch, M. J.; Trucks, G. W.; Schlegel, H. B.; Scuseria, G. E.; Robb, M. A.; Cheeseman, J. R.; Scalmani, G.; Barone, V.; Mennucci, B.; Petersson, G. A.; Nakatsuji, H.; Caricato, M.; Li, X.; Hratchian, H. P.; Izmaylov, A. F.; Bloino, J.; Zheng, G.; Sonnenberg, J. L.; Hada, M.; Ehara, M.; Toyota, K.; Fukuda, R.; Hasegawa, J.; Ishida, M.; Nakajima, T.; Honda, Y.; Kitao, O.; Nakai, H.; Vreven, T.; Montgomery, J. A., Jr.; Peralta, J. E.; Ogliaro, F.; Bearpark, M.; Heyd, J. J.; Brothers, E.; Kudin, K. N.; Staroverov, V. N.; Kobayashi, R.; Normand, J.; Raghavachari, K.; Rendell, A.; Burant, J. C.; Iyengar, S. S.; Tomasi, J.; M. Cossi, N. R.; Millam, J. M.; Klene, M.; Knox, J. E.; Cross, J. B.; Bakken, V.; Adamo, C.; Jaramillo, J.; Gomperts, R.; Stratmann, R. E.; Yazyev, O.; Austin, A. J.; Cammi, R.; Pomelli, C.; Ochterski, J. W.; Martin, R. L.; Morokuma, K.; Zakrzewski, V. G.; Voth, G. A.; Salvador, P.; Dannenberg, J. J.; Dapprich, S.; Daniels, A. D.; Farkas, Ö.; Foresman, J. B.; Ortiz, J. V.; Cioslowski, J.; Fox, D. J. *Gaussian 09*, Rev. A.1; Gaussian, Inc.: Wallingford, CT, 2009.
(50) Schäfer, A.; Huber, C.; Ahlrichs, R. Fully optimized contracted Gaussian basis sets of triple zeta valence quality for atoms Li to Kr. *J. Chem. Phys.* **1994**, *100*, 5829−5835.
(51) Dolg, M.; Stoll, H.; Preuss, H. Energy-adjusted ab initio pseudopotentials for the rare earth elements. *J. Chem. Phys.* **1989**, *90*, 1730−1734.
(52) Tozer, D. J.; Handy, N. C. Improving Virtual Kohn-Sham Orbitals and Eigenvalues: Application to Excitation Energies and Static Polarizabilities. *J. Chem. Phys.* **1998**, *109*, 10180−10189.

https://doi.org/10.1021/jacsau.1c00469
JACS Au 2022, 2, 197−203